

Edinburgh-2010/14

Step-scaling with off-shell renormalisation

R. Arthur¹ and P. A. Boyle¹

(RBC and UKQCD Collaborations)

¹*SUPA, School of Physics, The University of Edinburgh, Edinburgh EH9 3JZ, UK*

(Dated: May 4, 2019)

Abstract

We make use of twisted boundary conditions for off-shell Rome-Southampton renormalisation. This allows to define the vertex function precisely, at a fixed physical momentum that need not be one of the Fourier modes of a simulation. This definition includes choosing the orientation with respect to lattice axes, and so lattice artefacts including $\mathcal{O}(4)$ breaking then have a valid Symanzik expansion. Excellent statistical precision is afforded by volume plane-wave sources, enabling both a theoretically and statistically clean continuum limit to be taken. Thereafter all p^2 dependence can be unambiguously identified as continuum anomalous running.

The use of non-exceptional momenta has been found to greatly reduce the dependence of non-perturbative vertex functions on both mass and p^2 . We illustrate how this can be developed into a practical scheme for step-scaling the RI/SMOM approach with initial results. The size of the possible steps is continuous, rather than discrete allowing one to take arbitrarily small steps, and the scheme inherits from RI/MOM the property that it is easy to implement for general operators.

I. INTRODUCTION

The renormalisation of Lattice QCD matrix elements is an important topic for the phenomenological relevance of the field. This paper addresses two key limitations of the popular Rome-Southampton RI/MOM method[1]: firstly the entangled discretisation and perturbative truncation errors and secondly the rather low scale at which continuum perturbation theory is applied.

Phenomenology requires that scheme dependent QCD observables calculated within lattice QCD are converted to a perturbatively amenable scheme such as \overline{MS} . This is often done using an intermediate, regularisation invariant mom scheme (known as RI/MOM). The conversion of lattice results to the RI/MOM scheme has full, non-perturbative precision with the scale defined by the momenta used. Precision in the lattice results requires that the momentum scale used is well below the lattice cut-off, giving the high end of the Rome-Southampton momentum “window” condition:

$$\Lambda_{\text{QCD}}^2 \ll p^2 \ll \left(\frac{\pi}{a}\right)^2. \quad (1)$$

The perturbative conversion between RI/MOM (or SMOM in the case of non-exceptional kinematics) and \overline{MS} is known for many operators, and to as many as three loops. Perturbative accuracy is dependent on satisfying the lower inequality in Eq. (1). The error associated with the low end of the window depends on logarithms the physical momentum scale, while the high end converges as a power of the dimensionless momentum scale. The continuum extrapolation enabled by this work affords some tolerance to operating near the margins on the high side by extrapolating away discretisation errors. The step scaling proposed in this work is intended to raise the momentum scale into a more convergent perturbative regime.

The structure of the paper is as follows. In section II we summarise present current best practice for non-perturbative renormalisation. In section III we discuss the introduction of twisted boundary conditions in the valence sector for fermion vertex functions (III A), and define lattice kinematics (III B) with which intend to take the continuum limit (III C) for both exceptional and non-exceptional momenta. Our proposed step scaling scheme is based on these techniques, section III D.

We present data for the amputated vertex functions at a single lattice spacing in section IV A. In section IV C we demonstrate practicality using existing configurations to take the continuum limit for the first step in the step scaling programme.

II. BACKGROUND

The Rome-Southampton RI/MOM approach [1] involves a simple physically defined momentum scheme, albeit with particularly unphysical renormalisation conditions. For any given operator, \mathcal{O} , a momentum configuration for the vertex function of that operator is chosen. The renormalisation condition within any regularization scheme S is that the interacting amputated vertex function, when renormalised, is equal to the tree level operator at this momentum point. For example, for bilinears this is

$$\Lambda_{\mathcal{O}}^{S,ren}(p_1, p_2) = \frac{Z_{\mathcal{O}}^S}{Z_q} \Lambda_{\mathcal{O}}^S(p_1, p_2) = \mathcal{O}^{\text{tree}} \quad (2)$$

The original paper used the amplitude with

$$p_1 = p_2; q^2 = 0. \quad (3)$$

The approach facilitates the conversion between different schemes because all that is required in any given scheme S is a self-consistent calculation of the relevant scattering amplitude to some order. By virtue of the physical definition, one scheme can be a fully non-perturbative lattice calculation with some lattice action at non-zero lattice spacing. Thus, within the scaling window, Eq (1), a lattice simulation can be matched directly to continuum perturbation theory without use of ill-convergent lattice perturbation theory.

Studies with the original point source method did not resolve $\mathcal{O}(4)$ breaking a^2 lattice artefacts due to statistical imprecision. Different $\mathcal{O}(4)$ equivalent but $\mathcal{H}(4)$ distinct momentum configurations, given by different Fourier modes, were averaged together. When comparing different lattice spacings the coincidental numerology of which Fourier modes are available on the simulated lattices propagates into the continuum extrapolation. One should rather aim to take a controlled continuum limit in a^2 by picking precisely the same observable on each lattice spacing, and this implies using the same lattice momenta in the renormalisation.

A. Volume source NPR

The original method used a single point source for operator insertion. The volume source technique was developed by QCDSF [2]. The attraction here is to evaluate the amputated

vertex function with the operator insertion averaged over all L^4 lattice sites. When envisaging a series of steps, small statistical errors are imperative as error composition will inflate errors as a number of steps are taken.

We shall see it is easily possible to obtain 0.1% scale errors with volume source techniques, and even smaller if hundreds of configurations or larger volumes were used. With this statistical precision, and the selection of single specific Fourier modes, systematic effects like $\mathcal{O}(4)$ breaking lattice artefacts are visible and in fact are the dominant systematic error. These must be either included in the error analysis, or better yet addressed using the techniques of this paper.

We use i, j to represent colour indexes, and α, β to represent spin indexes. We define the four momentum source, used on a Landau gauge fixed configuration, as

$$\eta_k(x) = e^{ik_\mu x^\mu} \delta_{ij} \delta_{\alpha\beta}, \quad (4)$$

where the momenta are

$$k_\mu = n_\mu \frac{2\pi}{L}. \quad (5)$$

On a given gauge field $U_\mu(x)$ we solve

$$\sum_y M(x, y) G(y) = \eta(x), \quad (6)$$

and M is the Domain Wall fermion matrix [3]. One propagator inversion for each leg momentum is necessary, but this is more than offset by the gain in statistical accuracy. We select two independent momenta p_1 , and p_2 , and form phased propagators for each:

$$G'(x, p) = G(x, p) e^{-ip \cdot x} = \sum_y M^{-1}(x, y) e^{ip \cdot (y-x)}. \quad (7)$$

We form unamputated bilinear vertex functions for Dirac structure Γ :

$$\left[\sum_x \gamma_5 (G'(x, p_1))^\dagger \gamma_5 \Gamma G'(x, p_2) \right]_{ij, \alpha\beta}, \quad (8)$$

and also for four quark operators:

$$\sum_x (\gamma_5 (G'(x, p_1))^\dagger \gamma_5 \Gamma G'(x, p_2))_{ij, \alpha\beta} (\gamma_5 (G'(x, p_1))^\dagger \gamma_5 \Gamma G'(x, p_2))_{kl, \gamma\delta}. \quad (9)$$

Here, external colour and spin indexes are left free for off line amputation and projection.

B. Non-exceptional momentum

In the original RI/MOM kinematic a single gluon can carry all the hard momentum in the amplitude and infra-red effects such as pion pole effects in Λ_P and the B_K mixing matrix, and also spontaneous chiral symmetry breaking effects in Λ_S which fall only as $\frac{1}{p^2}$. Depending on the operator these effects have theoretically inferred non-trivial dependence on the valence quark mass that can complicate mass extrapolations, and in cases requires pion pole subtraction [1, 5–7].

RBC and UKQCD have developed the non-exceptional momentum SMOM kinematic point as a preferred matching condition [8]. A significant gain comes from the extra suppression of non-perturbative effects. The perturbative expansion must be calculated for non-exceptional momenta; this has been performed to one loop for bilinear operators [9] and for B_K [10]. Two recent publications have extended this to two loops for two different schemes for the quark mass [11, 12]. The non-exceptional kinematic point for bilinears has

$$p_1^2 = p_2^2 = (p_1 - p_2)^2. \quad (10)$$

RBC and UKQCD have found [8] that both momentum and mass dependence are simplified with non-exceptional kinematics. With this momentum flow, multiple hard gluons are required to create a soft sub-graph and non-perturbative infra-red effects such as spontaneous chiral symmetry breaking fall as a higher power $\frac{1}{p^6}$ [13]. Additionally, as our aim is to carefully study vertex functions whilst reducing the volume, we require a momentum scheme that is not sensitive to condensate physics.

C. Step scaling background

QCD perturbation theory at lattice scales is not rapidly convergent, and a means to increase this scale without applying brute force to raise the lattice cut-off is required.

Step-scaling [14, 15] is the natural approach to do this, where in a series of simulations the physical volume is reduced as the lattice spacing is reduced to enable the renormalisation scale to be raised without the cost inflation associated with application of brute force. This method has been well developed in the Schrödinger functional approach [14–16, 16–20]. A finite volume scheme based on Creutz ratios has also been recently developed [21]. In this paper we seek to develop a related approach based on the Landau gauge fixed RI/MOM

method. This approach will not tie the scale to the volume, and will therefore also avoid the need to fine tune bare couplings to precisely match a volume sensitive renormalised coupling between simulations.

In step scaling there is typically a renormalisation condition imposed that is physically defined in a fictional finite volume universe. In the case of the Schrödinger functional this is the coupling $\bar{g}(\frac{1}{L})$, at a scale L defined by the volume. A second simulation, at the same bare coupling, with larger volume sL then gives $\bar{g}(\frac{1}{sL}) = \Sigma(s, \bar{g}(\frac{1}{L}), \frac{a}{L})$. Here $s > 1$ is a scale factor, and is typically $s = 2$.

The continuum limit of Σ , and $\bar{g}(\frac{1}{sL})$ is taken while holding the measured coupling at the high scale $\bar{g}(\frac{1}{L})$ fixed. This defines the trajectory to the continuum limit as having the renormalised coupling lattice artefact free at the scale $\frac{1}{L}$, while the coupling at the low scale $\bar{g}(\frac{1}{sL})$ has some discretisation errors that are removed by taking this continuum limit. As $\bar{g}(\frac{1}{L})$ is held fixed, this is the observable quantity used to define the lattice spacing and volume.

Thus, the length scale of the quantity that determines the lattice spacing for the scale evolution function is reduced as the scale becomes shorter. The carefully defined trajectory to the continuum limit ensures the scales entering the step scaling function when consecutive steps are “stitched together” do indeed match up in the continuum limit. We intend to reproduce this feature in our method.

However, the quantity used to define the scaling trajectory, namely $\bar{g}(\frac{1}{L})$, is directly sensitive the volume. This requires fine tuning of β to *exactly* match the measured non-perturbative coupling – and hence to match volumes defined using $\bar{g}(\frac{1}{L})$ to set the scale – while taking the continuum limit. This is a fine tuning step that our proposal below avoids. We will both use a length scale significantly shorter than L to determine the trajectory to the continuum limit, and also keep the off-shell momentum scales hard enough that the physical volume should not be resolved and the calculation finite volume effect safe. Further the ultimate matching will be to standard infinite volume perturbation theory, as is usually the case for off-shell renormalisation.

D. Previous work on step scaling RI/MOM

The possibility of step scaling with RI/MOM has been previously studied [22], [23]. This work used a series of quenched configurations where the ratio of lattice spacings had been tuned to be precisely a factor of two to obtain aligned Fourier modes. This fine tuning is expensive in a dynamical simulation. Use of power counting and the Rome-Southampton scaling window was made, rather than controlled continuum extrapolation at fixed physical momentum. Free parameters for each operator were introduced to match the renormalisation constants for at different β 's corresponding to the (possibly non-perturbative) anomalous scaling of the operator with the lattice cut-off.

This excellent start was not easily developed into a practical technique. We believe that three technical advantages we have over this earlier attempt that will make the task more tractable.

The first reduces statistical errors greatly giving precision to the approach. The second renders mass dependence and infra-red behaviour in p^2 benign; this greatly assists with both chiral extrapolation and matching between ensembles, in addition to finite volume sensitivity. These were described above.

In the following section of the paper we also introduce the third advantage: using twisted boundary conditions [24] to select arbitrary four momenta [25–29], the direction of the scattering momenta can be kept fixed relative to lattice axes and arbitrary values of p^2 can be chosen. This is a Good Thing because it allows the same physical momenta according to the lattice symmetries $H(4)$ to be chosen on each ensemble, and the vertex function observable will only then have a normal Symanzik expansion for continuum extrapolation. The approach enables precise matching of momenta between ensembles, and precise continuum extrapolation.

III. FORMULATION

In the following subsections we motivate and then define the use of twisted boundary conditions in the context of off-shell renormalisation, define our momentum conventions, develop a framework for controlled continuum extrapolation and develop a step scaling approach.

A. NPR with twisted boundary conditions

In typical usage, the RI/MOM method uses data from a single lattice spacing, and power counting establishes a region of safe operation deemed to minimise the admixture of lattice artefacts and perturbative errors. It would be rather better to crisply separate the lattice artefacts by continuum extrapolation, and then to apply perturbative matching in the continuum limit.

However, conventional approaches use discrete Fourier modes, $p_i = \frac{2\pi}{L_i}n_i$, and we are not typically able to measure exactly the same physical momenta on different lattice spacings due to this Fourier constraint. Even were momenta found with matching p^2 , the $\mathcal{O}(4)$ breaking lattice artefacts typically differ [10].

In the continuum, by $O(4)$ symmetry, all momenta with equal magnitude but different directions are equivalent. On the lattice there is only $H(4)$ symmetry and, even in the infinite volume, only momenta related by $\pi/2$ rotations and reflections are equivalent. $G(p, p')$ will have a different $O(a^2)$ error term depending on the direction of the momentum, therefore unless a fixed orientation is chosen an extrapolation in p or a is not valid and there will be some poorly treated systematic error from treating the different directions as equivalent.

We now apply twisted boundary conditions to gauge fixed off-shell renormalisation to enable the arbitrary momentum to be used differing from a simulation with an exact Fourier mode by only finite volume effects. In order to simultaneously satisfy the constraint (10) and only use one momentum direction we propose choosing one kinematic satisfying (10) and use twisted boundary conditions [25–29], to vary the magnitude of the momentum.

The twisting technique has been used to insert arbitrary three-momenta in form factor calculations with the success demonstrated, for example, by the direct comparison of refs [30, 31] to refs [29, 32, 33]. which make use of the same configurations and action.

In this paper the technique is used to allow arbitrary four-momenta to be used [25], and hence allow to rigorously disentangle discretisation and perturbative truncation effects for the first time. Of course, the lattice artefacts are still present at finite lattice spacing but, up to finite volume effects, these become the *same* lattice artefact at each lattice spacing – not the case if different Fourier modes are used. The goal is to enable us to determine the non-perturbative anomalous running in the RI scheme in the continuum limit prior to the use of continuum perturbation theory.

Let the quark fields satisfy twisted boundary conditions $q(x + L) = e^{i\theta}q(x)$ and define

$$\tilde{q}(x) = e^{iBx}q(x) \quad (11)$$

with $B = \frac{\theta}{L}$ so that $\tilde{q}(x)$ satisfies periodic boundary conditions. This transformation changes the continuum Dirac operator:

$$D = (\not{\partial} + M) \rightarrow \tilde{D} = (\not{\partial} + i\not{B} + M) \quad (12)$$

\tilde{D} has inverse \tilde{S} and D has inverse S ; they are related by

$$S(x, y) = e^{iB(x-y)}\tilde{S}(x, y) \quad (13)$$

using translational invariance which we should recover after gauge averaging. However we never need $S(x, y)$ itself so no extra uncertainty arises. Let

$$\tilde{G}(z, p) = \sum_x \tilde{S}(z, x)e^{ipx} \quad (14)$$

then

$$\sum_z \tilde{D}(y, z)\tilde{G}(z, p) = e^{ipy} \quad (15)$$

So inverting the twisted Dirac operator (12) with a momentum source gives $\tilde{G}(z, p)$. Note that $\tilde{S}(z, x)$ satisfies periodic boundary conditions so in the source term, e^{ipy} , $p_\mu = \frac{2\pi n_\mu}{L_\mu}$ is a Fourier mode. $\tilde{G}(z, p)$ is related to $G(z, p)$ via,

$$\tilde{G}(z, p) = \sum_x e^{-iB(z-x)}S(z, x)e^{ipx} = e^{-iBz}G(z, p + B) \quad (16)$$

The propagator can be obtained from,

$$\sum_z e^{-ipz}\tilde{G}(z, p) = \sum_{z,x} e^{-i(p+B)(z-x)}S(z, x) = VS(p + B) \quad (17)$$

where V is the volume. Thus the net effect of twisted boundary conditions is to shift the momentum $p \rightarrow p + B$ where B is arbitrary. In order to compute the non-exceptional Green's functions observe,

$$\tilde{G}_\Gamma(p_1, p_2) = \sum_{x,y,z} e^{-ip_1(x-z)}\tilde{S}(x, z)\Gamma e^{-ip_2(z-y)}\tilde{S}(z, y) = \sum_z \gamma_5 e^{ip_1 z} \tilde{G}(z, p_1)^\dagger \gamma_5 \Gamma e^{-ip_2 z} \tilde{G}(z, p_2) \quad (18)$$

Using the inverse of (16) $\tilde{G}_\Gamma(p_1, p_2)$ is seen to be,

$$\tilde{G}_\Gamma(p_1, p_2) = \sum_{x,y} \gamma_5 e^{i(p_1+B_1)x} G(x, p_1+B_1)^\dagger \gamma_5 \Gamma e^{-i(p_2+B_2)y} G(y, p_2+B_2) = G_\Gamma(p_1+B_1, p_2+B_2) \quad (19)$$

We consider the values for p_1 , p_2 , B_1 and B_2 in the following subsection.

B. Kinematics

We select Euclidean momenta $p_1 = (-1, 0, 1, 0)$ and $p_2 = (0, 1, 1, 0)$ up to $H(4)$ symmetry operations. This configuration minimises $S^4 = \sum_i p_i^4$ which we take as measure of discretization errors, subject to the constraint that $p_1/p_2/(p_1 - p_2)$ be $H(4)$ equivalent momenta.

It is certainly possible to rotate some combination of p_x, p_y, p_z into the temporal direction breaking this $H(4)$ equivalence, and this would form an interesting possibility to demonstrate universality of the continuum limit in a later work.

The non-exceptional $p_1/p_2/(p_1 - p_2)$ kinematics can be represented by an equilateral triangle in momentum space with vertices lying on the p_x, p_y, p_z coordinate axes. Continuously dilating this triangle using twisted boundary conditions allows one to pick a fixed MOM observable as the lattice spacing is varied. We choose parallel twisting vectors $B_1 = (-\theta, 0, \theta, 0)$ for momentum p_1 and $B_2 = (0, \theta, \theta, 0)$ for p_2 . Varying θ lets us scan along the p^2 axis with fixed orientation of the $p_1, p_2, p_1 - p_2$ triangle.

The non-exceptional momenta are chosen to have small discretisation errors by spreading the power across multiple coordinate axes. In general for any non-exceptional configuration there will be $O(a^2)$ errors. As long as the direction is kept fixed the error term is a smooth function of $(ap)^2$. This means a smooth extrapolation to the continuum limit is possible no matter what the direction, because it is fixed. For exceptional momentum amplitudes we take vertex functions with p_1 on both legs.

C. Continuum extrapolation

Between different lattice spacings we compare only renormalised quantities and their ratios. This is quite natural as we desire to take the continuum limit of the product of a bare operator matrix element and its RI scheme renormalisation constant at some accessible scale p . The scaling factors for each operator to match between different β 's introduced in [23] are then not required. The aim of the latter part of this paper will be to raise, in the continuum limit, this scale p to one ($s^n p$ where s is a scale factor) where there is better perturbative convergence.

We eliminate Z_q via the vertex function of the (conserved) vector or axial currents:

$$R_{\mathcal{O}}(p, a, m) = \frac{\Lambda_A(p, a, m)}{\Lambda_{\mathcal{O}}(p, a, m)} = \frac{Z_{\mathcal{O}}(p, a, m)}{Z_A(p, a, m)} \quad (20)$$

and this ratio will be extrapolated to the chiral limit, to produce a massless step scaling function

$$Z_{\mathcal{O}}(a, p) = Z_A \lim_{m \rightarrow 0} R_{\mathcal{O}}(p, a, m) \quad (21)$$

where for convenience we use the vertex function of the local rather than conserved axial current and eliminate this with a previously computed Z_A . We then continuum extrapolate the product of $Z_{\mathcal{O}}$ with $\langle \mathcal{O} \rangle$:

$$\langle \mathcal{O} \rangle^{\text{ren}} = \lim_{a \rightarrow 0} \langle \mathcal{O} \rangle Z_{\mathcal{O}}. \quad (22)$$

This gives $\langle \mathcal{O} \rangle$ in the RI/MOM scheme for a scale determined by the physical momentum chosen which must be the same scale on all the lattices used to take the continuum limit.

We also consider computing the factor required to convert $\langle \mathcal{O} \rangle$ at scale p to scale sp where $s > 1$ is a scale factor. Let the term

$$\Sigma_{\mathcal{O}}(p, sp, a) = \lim_{m \rightarrow 0} \frac{R_{\mathcal{O}}(sp, a, m)}{R_{\mathcal{O}}(p, a, m)}, \quad (23)$$

and

$$\sigma_{\mathcal{O}}(p, sp) = \lim_{a \rightarrow 0} \Sigma_{\mathcal{O}}(p, sp). \quad (24)$$

In ratio, the anomalous evolution of bare lattice fields with a will cancel. $\sigma_{\mathcal{O}}(p, sp)$ will expand the scale dependence continuously around our physical match scale in the continuum limit for the RI scheme. We can then assess the degree to which the running around our match scale is perturbative without risk of confusion by possible lattice artefacts. Further, by picking a well defined amplitude as a function of a we remove ambiguity in taking the continuum limit that arises when selecting different Fourier modes for each value of β .

D. Step scaling scheme

Thus far we have demonstrated how to obtain a controlled Symanzik expansion for lattice amputated vertex functions, and thereby better control of lattice artefacts via continuum extrapolation. We now attempt to address perturbative errors associated with the low-end of the Rome-Southampton scaling window by raising the scale at which we match to perturbation theory.

In order to demonstrate that we can extend this to a practical step scaling scheme to suppress perturbative errors, we require several further pieces. Firstly, we will define non-perturbative evolution ratios that allow to successively higher momentum scales. For the scheme to be affordable it is necessary that it be able to operate in a small volume. For offshell amplitudes this is the case whenever the virtuality is too hard to resolve the finite volume

$$(ap)^2 \gg \left(\frac{\pi}{L}\right)^2. \quad (25)$$

Thus, for the purposes of step scaling, the window condition Eq (1) becomes

$$\left(\frac{\pi}{aL}\right)^2 \ll p^2 \ll \left(\frac{\pi}{a}\right)^2. \quad (26)$$

This latter condition is likely possible to meet using modest lattice volumes $L \leq 16$ at all stages of the calculation.

We will compute vertex functions on lattices at different values of beta with overlapping scaling windows. This will then enable the determination of a continuum step scaling function for some operator \mathcal{O} at a physical scale p^2 chosen in the window Eq (26) to that at a scale larger by a scale factor s . This is precisely $\sigma_{\mathcal{O}}(p, sp)$ from the previous section. Note that the approach represents a mass independent scheme.

For phenomenological application our aim is precise conversion of the continuum limit of the RI/SMOM scheme QCD matrix element at some rather infra-red momentum scale to \overline{MS} . This would better be done by a series of non-perturbative steps to a high scale, with perturbative conversion to \overline{MS} applied only where it is well convergent. For example,

$$\begin{aligned} \langle \mathcal{O}^{\overline{MS}}(\mu) \rangle &= \langle \mathcal{O}^{\text{SMOM}}(p) \rangle \\ &\times \sigma_{\mathcal{O}}^1(p, sp) \\ &\times \sigma_{\mathcal{O}}^2(sp, s^2p) \\ &\dots \\ &\times \sigma_{\mathcal{O}}^n(s^{n-1}p, s^n p) \\ &\times \left[1 + c^{\text{SMOM} \rightarrow \overline{MS}} \alpha_s(\mu = s^n p) \right]. \end{aligned} \quad (27)$$

It appears clear that Eq (26) can be satisfied at reasonable expense. For example 16^3 domain wall Fermion simulations will be inexpensive to the next generation of supercomputers; multiple such ensembles dedicated solely to the renormalisation of lattice operators are quite affordable. This is particularly helped by the relatively benign mass dependence of

non-exceptional momentum vertex functions. It is also clear that on these proposed small ensembles all hadronic quantities must be avoided to ensure finite volume safety of the analysis. For the determination of m_{res} , the PCAC is an operator relation and so it is immaterial whether a finite volume, or a physical pionic state is used to determine the ratio. Determining the lattice spacing (or more specifically the ratio of the lattice spacing to that of an earlier large volume simulation), in a finite volume safe manner is discussed below.

Here we have been somewhat vague about how the continuum limit of $\Sigma_{\mathcal{O}}^n(s^{n-1}p, s^n p, a)$ should be taken to obtain $\sigma_{\mathcal{O}}^n(s^{n-1}p, s^n p)$. Since we plan to reduce the volume successively, a different definition of the lattice spacing should be used to define the momentum scale $s^n p$ entering $\Sigma_{\mathcal{O}}^n(s^{n-1}p, s^n p, a)$ than is used to define the same momentum scale $s^n p$ in the next step $\Sigma_{\mathcal{O}}^{n+1}(s^n p, s^{n+1}p, a)$. The two distinct trajectories to the continuum limit must be chosen in a way that guarantees to agree on this scale in the continuum limit when we multiply $\sigma_{\mathcal{O}}^n(s^{n-1}p, s^n p) \times \sigma_{\mathcal{O}}^{n+1}(s^n p, s^{n+1}p)$. In the Schrödinger functional method this is done by fine tuning (i.e. constraining) the low scale coupling at each lattice spacing step $n + 1$ to match the continuum limit of the high scale coupling obtained from the previous step.

E. Trajectory to continuum limit

Identification of the ratio of lattice spacings of ensembles with different values of the bare coupling $\beta = \frac{6}{g^2}$ in our step scaling scheme is a challenge as we have deliberately forsaken the approach of using the finite volume to determine a renormalised coupling. We require a family of scale determining quantities $\{q_i(x)\}$ for which we must arrange that momentum scales in the corresponding sequence of scale evolution functions “joins up” in the continuum limit. It remains essential that the determination of ratios of lattice spacings, as we change β , be based on increasingly short distance quantities to ensure we can reduce the lattice volume as we proceed.

We will determine the scale from non-perturbatively determined quantities that are appropriate continuous functions of distance or momentum. These will be kept distinct from the object that is renormalised, and the length scale involved will be kept significantly smaller than the volume. The continuum ratio of successive quantities in the sequence $\left(\frac{q_{n-1}(a)}{q_{n-2}}\right)^{\text{cont}}$ will be determined non-perturbatively as we proceed and used to ensure our successive steps are “joined up”.

At step n we will determine:

$$\sigma_{\mathcal{O}}^n(s^{n-1}p, s^n p) = \lim_{a \rightarrow 0} \Sigma_{\mathcal{O}}^n(s^{n-1}p, s^n p, a) \Big|_{\frac{s^n p}{q_n(a)} = \frac{s^n p}{q_{n-1}^{\text{cont}}}\left(\frac{q_{n-1}}{q_n}\right)^{\text{cont}}}, \quad (28)$$

$$\left(\frac{q_{n+1}}{q_n}\right)^{\text{cont}} = \lim_{a \rightarrow 0} \left(\frac{q_{n+1}(a)}{q_n(a)}\right)^{\text{cont}}, \quad (29)$$

where the constraint on our trajectory to the continuum limit

$$\frac{s^n p}{q_n(a)} = \frac{s^n p}{q_{n-1}^{\text{cont}}}\left(\frac{q_{n-1}}{q_n}\right)^{\text{cont}} \quad (30)$$

requires that the momentum scale $s^n p$ set using quantity $q_n(a)$ at each lattice spacing has to agree, in the continuum limit, with a trajectory using $q_{n-1}(a)$ instead. The condition depends only on quantities determined in previous steps.

Ultimately this will become difficult as all dependence on lattice spacing becomes logarithmic and precision quantities are required; however, there may also be less appropriate but expedient choices that enable immediate progress for a few steps away from our relatively coarse simulations. We consider two possibilities.

1. *Static potential*

We note the static potential has been measured successfully over a large range of length scales in the quenched approximation with the Wilson gauge action [34]. This involved the use of a shorter length scale $r_c \simeq 0.26\text{fm}$ than the more common $r_0 \simeq 0.48\text{fm}$ [35]. This calculation also interesting because it successfully fits $\log \frac{a}{r_0}$ as a polynomial in β . Such an approach may ultimately assist continuing lattice spacing determinations to increasingly fine and small volume simulations.

We consider a sequence of scales, of the same class as the Sommer scale

$$r_n^2 F(r_n) = C_n. \quad (31)$$

The Sommer scale r_0 takes

$$C_0 = 1.65 \quad (32)$$

Thus a step scaling scheme with scale factor s can then be defined choosing $p_n = s^n p$ and $r_n = \frac{r_0}{s^n}$ as follows:

- Determine $\sigma(p_0, p_1)$ in continuum limit holding $r_0 p_0$ fixed such that $r_0^2 F(r_0) = C_0$

- Determine $C_1 = \frac{r_0^2}{s^2} F(\frac{r_0}{s})$ in continuum limit holding r_0 fixed
- Decrease L by $\simeq \frac{1}{s}$ without fine tuning
- Determine $\sigma(p_1, p_2)$ in continuum limit holding $r_1 p_1$ fixed such that $r_1^2 F(r_1) = C_1$
- Determine $C_2 = \frac{r_1^2}{s^2} F(\frac{r_1}{s})$ in continuum limit holding r_1 fixed
- Decrease L by $\simeq \frac{1}{s}$ without fine tuning
- etc...

Following a rule of thumb that $r < \frac{L}{3}$ for the static potential should ensure finite volume safety and enable simulation down to $L \simeq 0.75\text{fm}$ when using scales similar to r_c to set the scale. Eventually this will become imprecise when entering a region where the potential runs logarithmically. However we believe a substantial benefit is already achievable prior to addressing this issue.

2. Vertex function form factors

In principle, we can use the momentum dependence of the off-shell vertex functions themselves to match the lattice scales between different ensembles. This may be assisted by the improved techniques of this paper, and particularly the tunable momentum scale at which perform the matching allows to select the length scale from which the lattice spacing is set. This will be the subject of a further study.

IV. RESULTS

We use the domain wall fermion action [3], and $16^3 \times 32$ ensembles with $L_s = 16$ and with the Iwasaki gauge action [4]. We use two ensemble sets in this paper, with $\beta = 2.13$ and $\beta = 2.23$. The $\beta = 2.13$ ensembles were studied extensively in Ref. [36]. The three $\beta = 2.13$ 16^3 ensembles used in this section have strange quark mass $m_h = 0.04$ and degenerate light quark masses $m_l = 0.01, 0.02, 0.03$. The second ensemble set with $\beta = 2.23$ is not previously published and was used as part of an unpublished parameter search, made in the style of [37, 38], prior to our 32^3 simulations [39] which lie nearby in parameter space. There are

two ensembles with $m_h = 0.04$ and $m_l = 0.01, 0.02$. There are around 2000 trajectories in these ensembles.

For $\beta = 2.13$ the extrapolations to $m_q = -m_{res}$ were made with $m_{res} = 0.00305$, $Z_A = 0.7161(1)$, and the lattice spacing was taken as $a^{-1} = 1.729$ GeV [40]. We find in this paper that $\beta = 2.23$ corresponds to an inverse lattice spacing of around $a^{-1} \simeq 2.14$ GeV, with residual mass $m_{res} \simeq 10^{-3}$, and we estimate $Z_A = 0.740$ by interpolating between nearby values for β . This is not ideal, but adequate for the purposes of this demonstration.

All of the vertex function data was computed using the volume source method with twisted boundary conditions method as described in section III A using 20 gauge configurations for each mass, see tables I and II.

am_q	Range	Δ
0.03	800 - 2320	80
0.02	1000 - 2520	80
0.01	1000 - 2520	80

Table I: $\beta = 2.13$ lattice giving the range of molecular dynamics time and the separation Δ between gauge configurations used in this work. Because so few configurations are needed with the volume averaging a large Δ was chosen to minimise auto-correlation effects.

am_q	Range	Δ
0.02	1000 - 1760	40
0.01	1240 - 2000	40

Table II: $\beta = 2.23$ lattice giving the range of molecular dynamics time and the separation Δ between gauge configurations used in this work. Because so few configurations are needed with the volume averaging a large Δ was chosen to minimise auto-correlation effects.

A. Vertex functions with twisted boundary conditions at a single lattice spacing

In this section we focus on the data obtained using the $\beta = 2.13$ ensembles and display the quality of data obtained on a single lattice spacing.

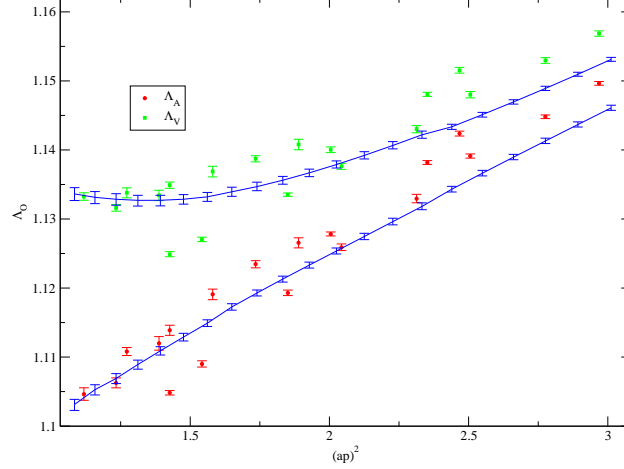


Figure 1: The axial (red) and vector (green) vertices computed at exceptional momentum with a volume source at fixed quark mass $m_q = 0.03$ on the $\beta = 2.13$ lattice, using 10 configurations, see Section IV A for more details. The red and green points are computed using different Fourier momenta, with different directions, as a source. The blue data is computed with twisted boundary conditions using the momentum sources $(0, 2, 2, 0)$ and $(0, 3, 3, 0)$ with twisting angles $\frac{\pi}{L}(\frac{n}{8})$ where $n = -3, -2, \dots, 12$ to get the desired momentum. The twisting has completely eliminated the $O(4)$ breaking scatter that was present using the Fourier mode sources.

With $G_\Gamma(p_1, p_2)$ and $G(p_1, p_2)$ computed as above we define the amputated Green's function as,

$$\Pi_\Gamma(p) = (G^{-1}(p_1, p_1)G_\Gamma(p_1, p_2)\gamma_5[G^{-1}(p_2, p_2)]^\dagger\gamma_5) \quad (33)$$

where $p^2 = p_1^2 = p_2^2 = (p_1 - p_2)^2$, and we take $q = p_1 - p_2$. The bare vertex amplitudes are then obtained by projecting the amputated Green's functions onto their tree level values,

$$\Lambda_O = \frac{1}{12}Tr(\Pi_O P_O) \quad (34)$$

Figure 1 contains an comparison of the traditional volume averaged Fourier mode technique to our new twisted boundary condition NPR technique. $O(4)$ breaking lattice artefacts produce a large scatter in the data using the traditional approach and this is scatter completely removed by the technique. Of course, lattice artefacts are still present and of the same size, but the key point is that we can now vary β while looking at the same off-shell momentum in order to extrapolate these away in the continuum limit.

For the exceptional kinematic configuration we use the projectors of [8] and the pertur-

bative running and matching calculated in [41] for mass and [42] for the tensor current. For \mathcal{O}_{VV+AA} we use the results of [43, 44]. We denote these exceptional momentum schemes RIMOM.

For non-exceptional kinematics we compare the two schemes introduced in [9]. The first is the scheme of [9] which corresponds to choosing projectors $\not{q}q_\mu$ for the vector vertex function and $\not{q}q_\mu\gamma_5$ for the axial vertex function. We denote this scheme SMOM- \not{q} . The second uses γ_μ and $\gamma_\mu\gamma_5$ for vector and axial vertex functions, we refer to this scheme as SMOM- γ_μ . The one-loop matching and two-loop anomolous dimensions for tensor current and mass are given in [9]. These results have recently been extended to two loop matching and three loop anomolous dimensions [11, 12]. For \mathcal{O}_{VV+AA} we use several unpublished new schemes and perturbative results by Sachrajda and Sturm [10], and we thank them for their private communications.

Figure 2 displays the projections of all the Dirac structures analysed in this paper for the $\beta = 2.13$ ensemble, and for both non-exceptional and exceptional. We will return study each of these structures in turn and in more detail below.

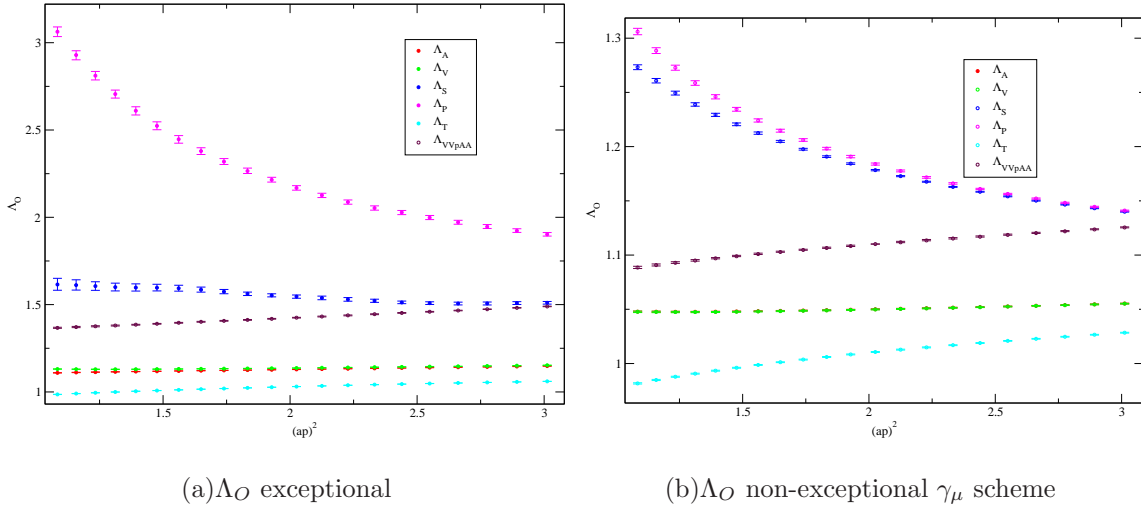


Figure 2: The Vector, Axial Vector, Scalar, Pseudoscalar, Tensor and four quark operator \mathcal{O}_{VV+AA} vertex functions (Λ_O) on the $\beta = 2.13$ lattice. Exceptional momentum at $m_q = 0.01$, non-exceptional momentum is presented in the chiral limit. The exceptional momentum configuration used $p_1 = p_2 = (0, 2, 2, 0)$ as the base Fourier momentum, non-exceptional momentum used $p_1 = (0, 2, 2, 0)$ and $p_2 = (-2, 0, 2, 0)$. Note the great reduction in chiral symmetry breaking effects ($\Lambda_A - \Lambda_V$ and $\Lambda_S - \Lambda_P$) at non-exceptional momentum.

We wish to eliminate the wavefunction renormalisation by taking ratios $\frac{\Lambda_A}{\Lambda_O}$ and where Λ_A is the vertex function of the local axial current, and its renormalisation is eliminated using Z_A previously determined from the ratio of matrix elements the local axial current and of the conserved axial current. From the Ward identities in the limit of small mass and large momentum we should find that $Z_V \simeq Z_A$ and $Z_S = Z_P$. These are well supported by our data for non-exceptional momentum, but over our momentum range not held for exceptional momentum configurations. In order to compare with previous results we adopt, for non-exceptional momentum, the strategy of [8] eliminating the quark field renormalisation using

$$\frac{Z_q}{Z_A} = \frac{1}{2}(\Lambda_A + \Lambda_V), \quad (35)$$

where factors of Z_A are then multiplied out using a previously calculated value. For exceptional data this matches central value conventions with [8] where the difference between taking $\frac{Z_q}{Z_A} = \frac{1}{2}(\Lambda_A + \Lambda_V)$, and $\frac{Z_q}{Z_A} = \Lambda_A$ was used as a systematic error.

For the non-exceptional case we use simply $\frac{Z_q}{Z_A} = \Lambda_A$. In this case, we have

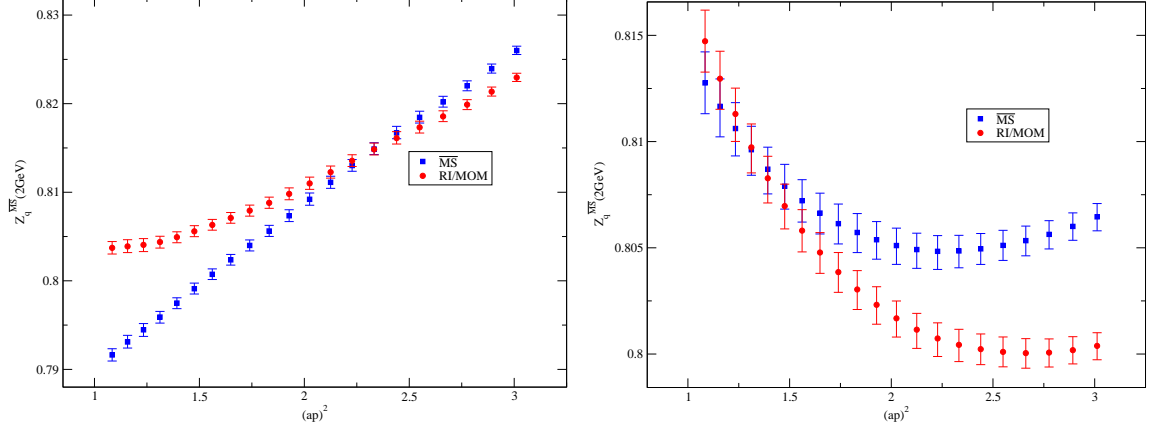
$$Z_m Z_A = \frac{\Lambda_S}{\Lambda_A}, \quad (36)$$

$$\frac{Z_T}{Z_A} = \frac{\Lambda_A}{\Lambda_T}, \quad (37)$$

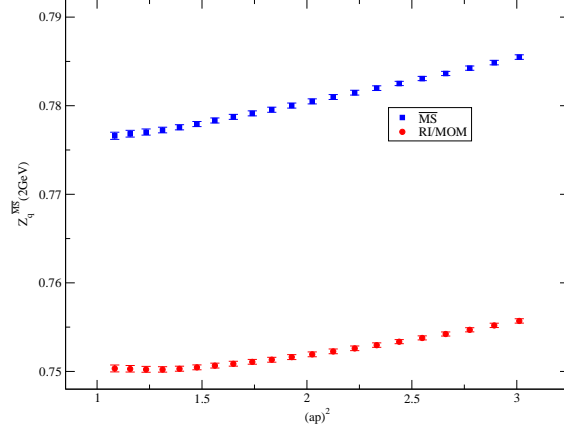
$$Z_{B_K} = \frac{Z_{\mathcal{O}_{VV+AA}}}{Z_A^2} = \frac{\Lambda_A^2}{\Lambda_{\mathcal{O}_{VV+AA}}}. \quad (38)$$

Our results for RIMOM, SMOM- q , and SMOM- γ_μ schemes for the wave function renormalisation determined from the axial current vertex function (non-exceptional) and average of axial and vector vertex functions (exceptional) are displayed in figure 3. Here, the running at this lattice spacing is poorly described by continuum perturbation theory, and is associated with the momentum dependence of the exponent for binding of light modes in the fifth dimension in the domain wall formulation [45]. We note that this Z_q is cancelled in the ratios above when treating other operators. Naturally, one expects that such discretisation effects will be removed if a controlled continuum limit is taken, and this will be revisited in later sections.

Figures 4, 5, and 6 display the corresponding data for the mass, tensor current and four quark operator \mathcal{O}_{VV+AA} relevant for B_K . As promised, the data is extremely precise and $\mathcal{O}(4)$ breaking discretisation effects do not introduce scatter in the data as the momentum is changed because we are always selecting the same lattice momentum with our twisted



(a) $Z_q^{\overline{MS}}(2\text{GeV})$ determined via RI/MOM (h) $Z_q^{\overline{MS}}(2\text{GeV})$ determined via SMOM- g scheme



(c) $Z_q^{\overline{MS}}(2\text{GeV})$ determined via SMOM- γ_μ scheme

Figure 3: Chiral limits of $Z_q = \frac{Z_A}{2}(\Lambda_A + \Lambda_V)$ on the $\beta = 2.13$ lattice in the RI/MOM scheme (red), and with the perturbative running divided out (blue). For the SMOM schemes we use $Z_q = \frac{Z_A}{\Lambda_A}$. For comparison to [8], linear dependence on $(ap)^2$ which is fitted and extrapolated to zero with fit range $2 < (ap)^2 < 3.2$. We note that this is in danger of extrapolating perturbative errors into the infrared, and in this work rather advocate taking the continuum limit from determinations using a fixed non-zero physical momentum, for example $p^2 = (2\text{GeV})^2$, to eliminate discretisation errors. This momentum should be high to ensure minimal perturbative error. The running of Z_q contains strong lattice artefacts for DWF and is opposite to the continuum running. We find later that in the continuum limit this becomes consistent.

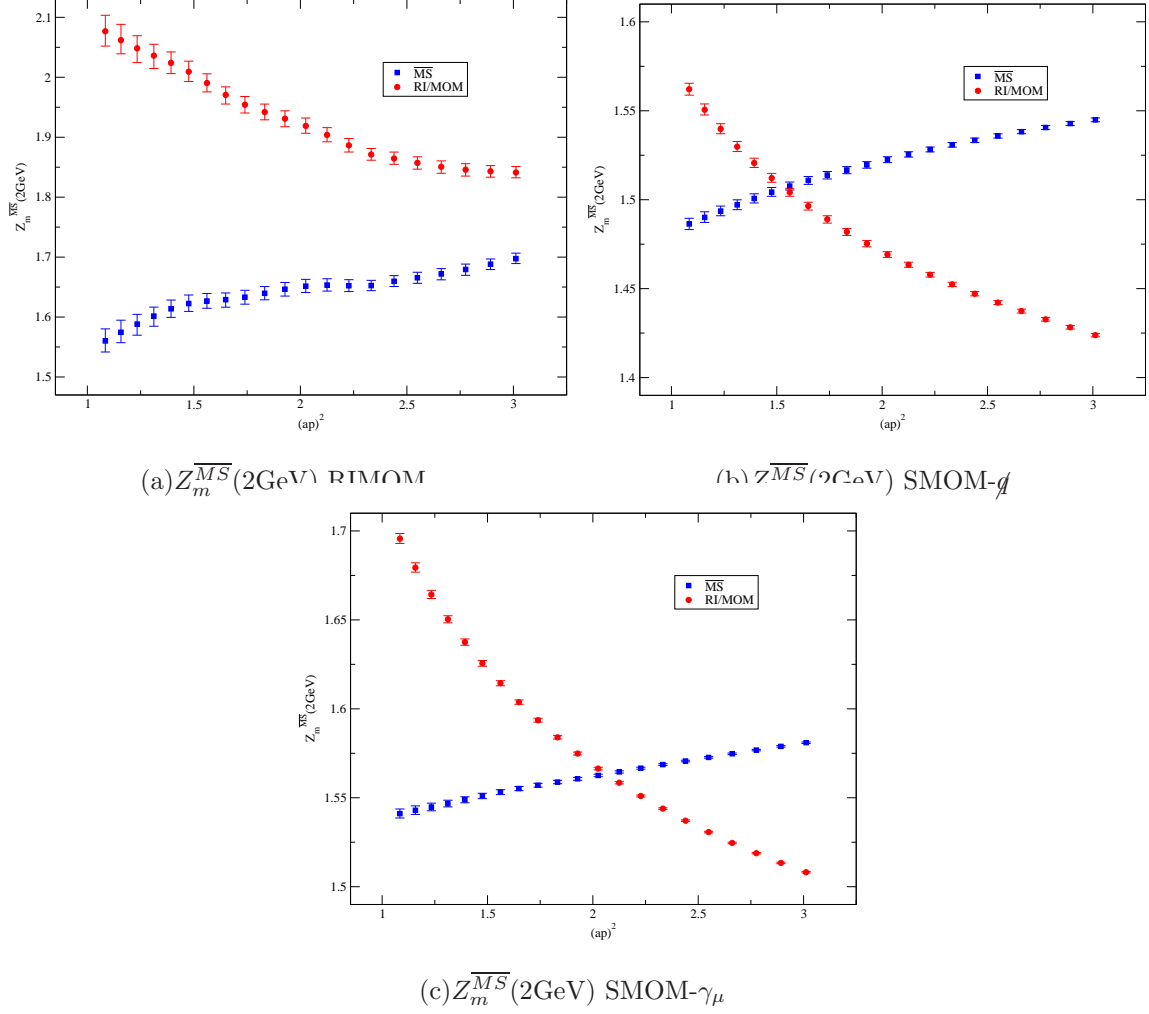


Figure 4: Quark mass renormalization in the chiral limit: (a) exceptional momentum ($Z_m = \frac{2}{Z_A} \frac{\Lambda_S}{\Lambda_A + \Lambda_V}$), and (b,c) non-exceptional momentum ($Z_m = \frac{\Lambda_S}{Z_A \Lambda_A}$) on the $\beta = 2.13$ lattice. For comparison to [8], linear dependence on $(ap)^2$ which is fitted and extrapolated to zero with fit range $2 < (ap)^2 < 3.2$. We note that this is in danger of extrapolating perturbative errors into the infrared, and in this work rather advocate taking the continuum limit at non-zero momentum to eliminate discretisation errors. This momentum should be high to ensure minimal perturbative error.

boundary conditions. Errors are at the 0.1% level even on this relatively small volume and with only twenty configurations.

Table IV shows our results compared with the results of Ref [8] after following the same procedure of extrapolation to $p^2 = 0$ and after converting to the \overline{MS} scheme at 2 GeV. This procedure is flawed, and we note that this is in danger of extrapolating perturbative

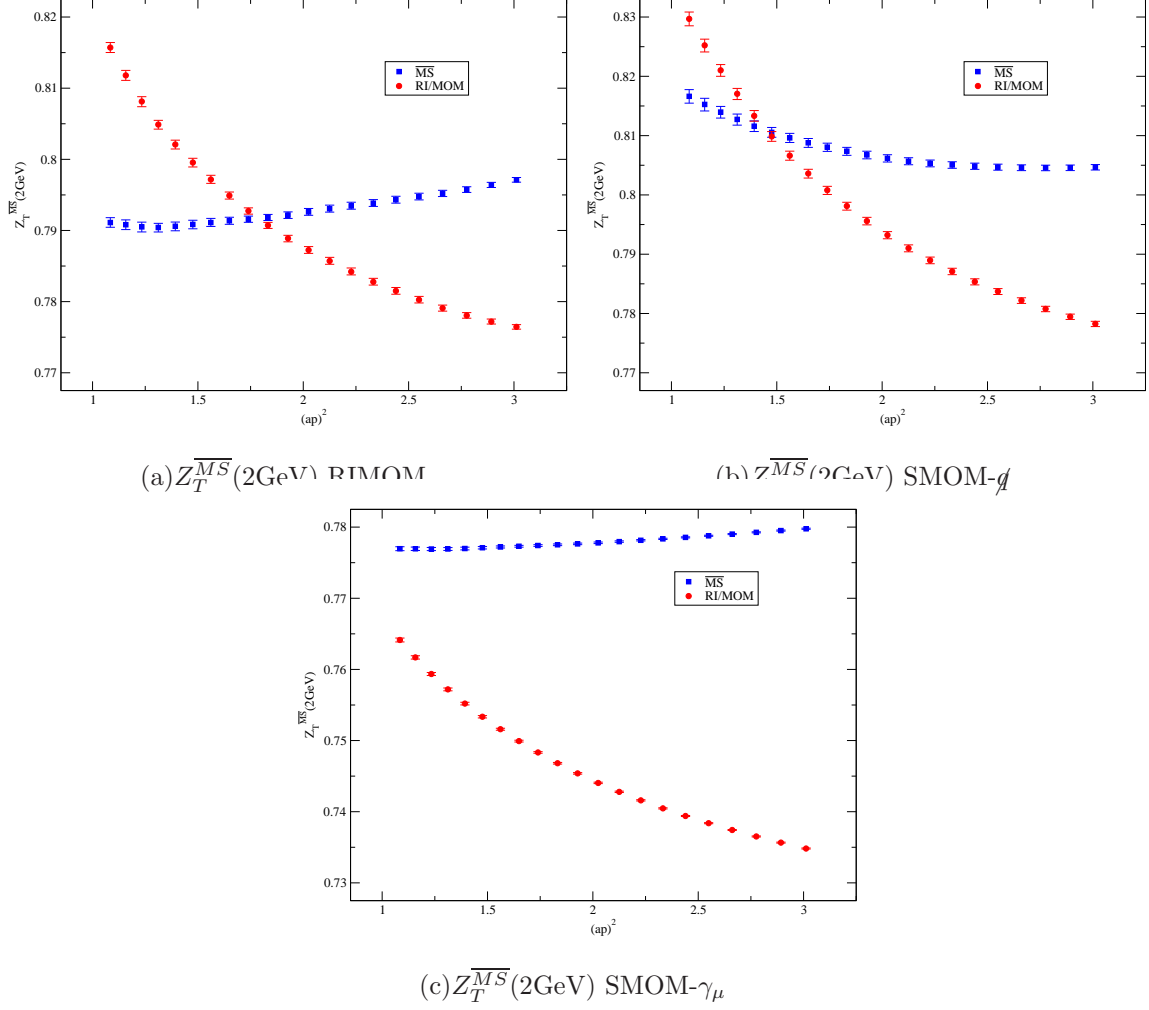


Figure 5: Tensor current renormalization in the chiral limit: (a) exceptional momentum ($Z_T = Z_A \frac{\Lambda_A + \Lambda_V}{2\Lambda_T}$), and (b,c) non-exceptional momentum ($Z_T = Z_A \frac{\Lambda_A}{\Lambda_T}$) on the $\beta = 2.13$ lattice. For comparison to [8], linear dependence on $(ap)^2$ which is fitted and extrapolated to zero with fit range $2 < (ap)^2 < 3.2$. We note that this is in danger of extrapolating perturbative errors into the infrared, and in this work rather advocate taking the continuum limit at non-zero momentum to eliminate discretisation errors. This momentum should be high to ensure minimal perturbative error.

errors into the infrared. In the next section we show rather how to take the continuum limit at non-zero momentum to eliminate discretisation errors. These numbers are thus for comparison only, and constitute a check and a demonstration of the precision that is possible using the techniques of this paper. The numbers do not represent an attempt to improve on previous estimates of renormalization constants for the RBC/UKQCD domain

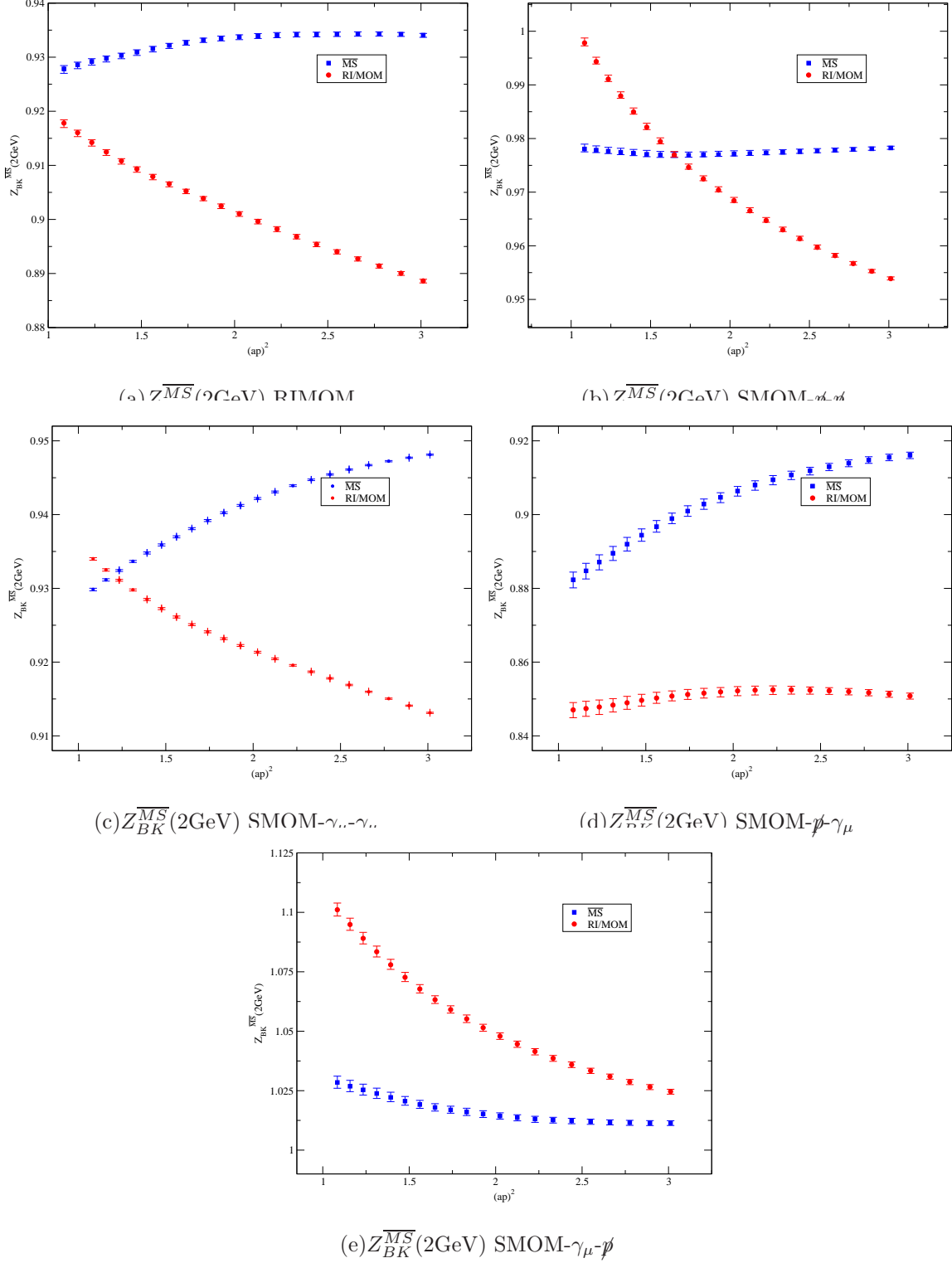


Figure 6: Four quark operator \mathcal{O}_{VV+AA} renormalization in the chiral limit: (a) exceptional momentum ($Z_{B_K} = \frac{1}{4} \frac{(\Lambda_A + \Lambda_V)^2}{\Lambda_{\mathcal{O}_{VV+AA}}}$), and (b-e) non-exceptional momentum ($Z_{B_K} = \frac{\Lambda_A^2}{\Lambda_{\mathcal{O}_{VV+AA}}}$) on the $\beta = 2.13$ lattice. For comparison to [8], linear dependence on $(ap)^2$ which is fitted and extrapolated to zero with fit range $2 < (ap)^2 < 3.2$. We note that this is in danger of extrapolating perturbative errors into the infrared, and in this work rather advocate taking the continuum limit at non-zero momentum to eliminate discretisation errors. This momentum should be high to ensure minimal

wall programme. The physical RBC-UKQCD predictions will be updated using the methods of this paper techniques in later works, where we will also use step scaling to raise the momentum scale to minimise perturbative error.

Z_O	Ref: [8]	RIMOM (extrap)	RIMOM	SMOM- q	SMOM- γ_μ
Z_q	0.7726(48 + 150)	0.7753(15)	0.79605(63)	0.8035(10)	0.77744(31)
Z_m	1.656(30 + 83)	1.483(28)	1.546(15)	1.5073(26)	1.5405(18)
Z_T	0.7950(34 + 150)	0.7962(13)	0.80339(62)	0.80626(73)	0.77768(20)

Table III: The quark field, mass and tensor current renormalization constants in \overline{MS} at $2(GeV)$. Error in the first column is (stat + sys) error in the other columns statistical only. Note this work used 20 configurations at each mass whereas [8] used 300 point source measurements on 75 configurations. The third column uses the value extrapolated to zero for comparison with the results of [8]. The others use simple interpolation to obtain the value at $p^2 = 2GeV$

Ref: [8]	RIMOM (extrap)	RIMOM	SMOM- (q,q)	SMOM- (γ_μ, γ_μ)	SMOM- (q, γ_μ)	SMOM- (γ_μ, q)
0.9276(52 + 220)	0.93330(73)	0.92994(54)	0.97737(59)	0.93406(60)	1.0233(21)	0.8903(19)

Table IV: BK renormalization constant with same parameters as above. The extrapolated RIMOM is for comparison with [8] the rest of the measurements use the interpolated value at $p^2 = 2GeV$.

B. Scale determination in a small volume

Determining the lattice spacing for our $\beta = 2.23$ ensemble is a useful test case for the methods of section III E.

As a preliminary we have calculated r_C for our 16^3 lattices. We compute timelike Wilson loops with four hits of APE smearing, smearing parameter 2.5, in the spatial direction. The tree level improvement of [34] is here required for the Iwasaki gluon action. We compute the tree level Wilson loop using code developed in [46] to obtain Table V where the potential includes the self energy part.

$$aV(\vec{R}a) = - \lim_{T \rightarrow \infty} \frac{1}{W(\vec{R}, T)} \frac{dW(\vec{R}, T)}{dT} = C_F V(\vec{R}) g^2 + O(g^4) \quad (39)$$

\vec{R}	V_W	V_I
(1,0,0)	0.166667	0.08963(1)
(2,0,0)	0.209842	0.12569(2)
(3,0,0)	0.225186	0.13879(3)
(4,0,0)	0.232442	0.14506(4)
(5,0,0)	0.236630	0.14878(4)
(6,0,0)	0.239366	0.15133(5)
(7,0,0)	0.241300	0.15318(5)
(8,0,0)	0.242742	0.15456(5)

Table V: V_W is the static potential tree level part with the Wilson gluon action, V_I uses the Iwasaki gluon action. As R tends to infinity the difference between successive terms for Wilson and Iwasaki actions (the force) is the same since the self energy part cancels and the two actions reproduce the same IR physics.

By demanding

$$F(r_I) = (V(r) - V(r - a))/a = F_{tree} = \frac{1}{4\pi r_I^2} \quad (40)$$

we solve for r_I using Table V. This approach leads to much reduced lattice $O(a^2)$ errors [34] [47]. Further, using the force instead of the potential removes the self energy part and reduces the linear term, σr , to a constant. Fitting the Cornell potential to find r_C requires σ . However, σ is dependant on the long distance behaviour of $V(r)$, and to constrain it one has to sample large r . When fitting to the force, r_C can be obtained without including large distance data in the procedure, and r_C computed this way is a finite volume safe observable with which to determine the lattice spacing.

In order to extract $V(r)$ from the average Wilson loops $\langle W(r, t) \rangle$ we first plot the effective potential

$$\log\left(\frac{\langle W(r, t+1) \rangle}{\langle W(r, t) \rangle}\right) \quad (41)$$

as a function of t . The largest value of r used in this analysis is $4a$. Excited state contamination and statistical noise are problematic, and we use the 'black box' method [48] to define an improved effective mass that takes account of the first excited state. This allows us to extend t_{min} to $t = 3$ which gives a significant error reduction compared to the usual effective mass. On the $\beta = 2.13$ lattice we use 600 configurations for each mass, each configuration

rotated to use 4 different time directions. For $\beta = 2.23$ we use 750 configurations per mass and again rotate the time direction.

The equation $r^2 F(r) = C$ has solutions in the range of our data for $C \in (0.6, 2.0)$. Lower values give more accurate r_C but these are likely to have large finite a errors. For any C however $\frac{r_C/a_{2.13}}{r_C/a_{2.23}}$ should be constant, we plot this ratio as a function of C in figure 8 and determine $C > 1.4$ is appropriate and gives the value for the ratio of lattice scales,

$$R_a^2 = \frac{(a_{2.23})^2}{(a_{2.13})^2} = 0.652(21) \quad (42)$$

This implies a lattice spacing of $a^{-1} \simeq 2.14$ GeV for the $\beta = 2.23$ ensembles.

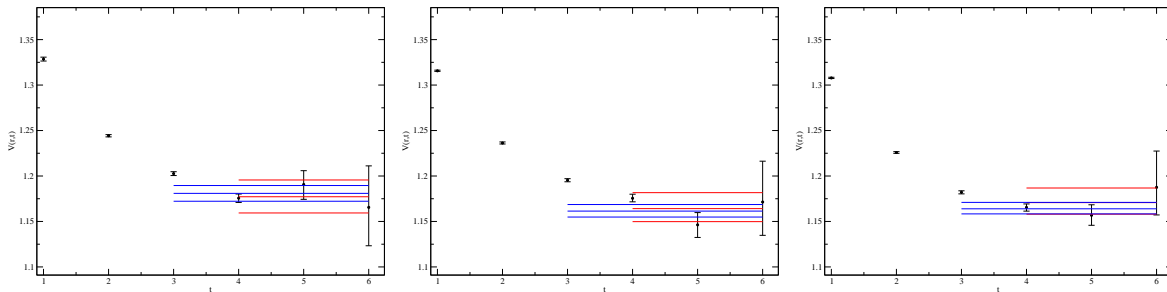


Figure 7: Effective mass plots for (left to right) $m = 0.03$, $m = 0.02$, $m = 0.01$ on the $\beta = 2.13$ lattice at $r = 4a$. Datapoints are computed via equation 41. The red constant is obtained from a fit over the last three datapoints. The blue is from the black box method with $t_{min} = 3$.

We propose below a scale factor $s = 1.5$, and believe that at least two iterations of step scaling should be possible based only on the static potential. However, the static potential displays percent scale errors even with many configurations and finding a more precise alternative would certainly be good in any case.

C. Continuum limit scale evolution functions

Following equation 24 we can compute $\sigma_O(p, sp)$ using two lattice spacings. We consider the evolution of renormalisation constants Z_q , Z_m , Z_T , and Z_{B_K} in both the exceptional and the non-exceptional kinematic schemes. We choose $p \simeq 2(\text{GeV})$ and compute $\sigma_O(p, sp)$ as a function of s .

Because of the very smooth p^2 dependence of the vertex functions computed with twisted boundary conditions we can perform a simple interpolation to match values of p^2 on each

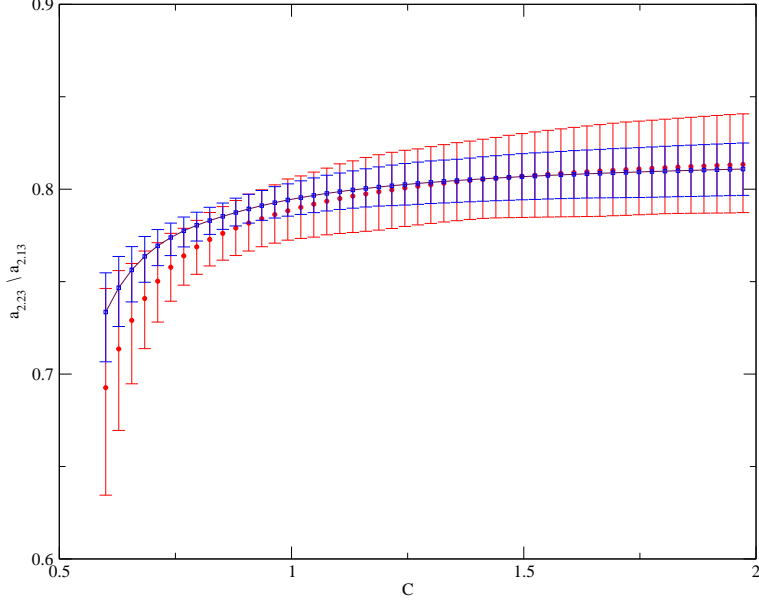


Figure 8: The ratio $\frac{r_C/a_{2,13}}{r_C/a_{2,23}}$ as a function of C . The red data is computed using the effective mass 41 $t_{min} = 4$ and the blue uses the black box method with $t_{min} = 3$, and gives the same value but with significantly smaller error.

lattice. One could in principle simulate at the same physical momentum on each lattice by choosing the twisting angles appropriately, however since the interpolation introduced only a very small uncertainty this is not necessary.

For each operator we can now evaluate $\Sigma_O(p = 2\text{GeV}, sp, a^{-1} = 1.729\text{GeV})$ and $\Sigma_O(p = 2\text{GeV}, sp, a^{-1} = 2.14\text{GeV})$. Linear extrapolation in a^2 with only two datapoints is not as robust as one might like, but certainly suffices to demonstrate the method. Using this, we can obtain the continuum limit step scaling function $\sigma_O(p = 2\text{GeV}, sp)$ for the quark field (figure 9), mass (figure 10), tensor current (figure 11), and the four quark operator \mathcal{O}_{VV+AA} (figure 12). With an appropriate third and smaller lattice spacing using a correspondingly smaller volume, we could similarly determine the next step, evolving from 3 GeV to 4.5 GeV.

Figure 9 is especially important. In the γ_μ scheme at exceptional and non-exceptional momenta and finite lattice spacing the running of Z_q is in the opposite direction to the perturbative prediction, however the correct running behaviour is recovered in the continuum limit. The determination of Z_q with domain wall fermions displays the momentum dependence of the exponent $\alpha(p)$ of localisation in the fifth dimension [45]. As shown here,

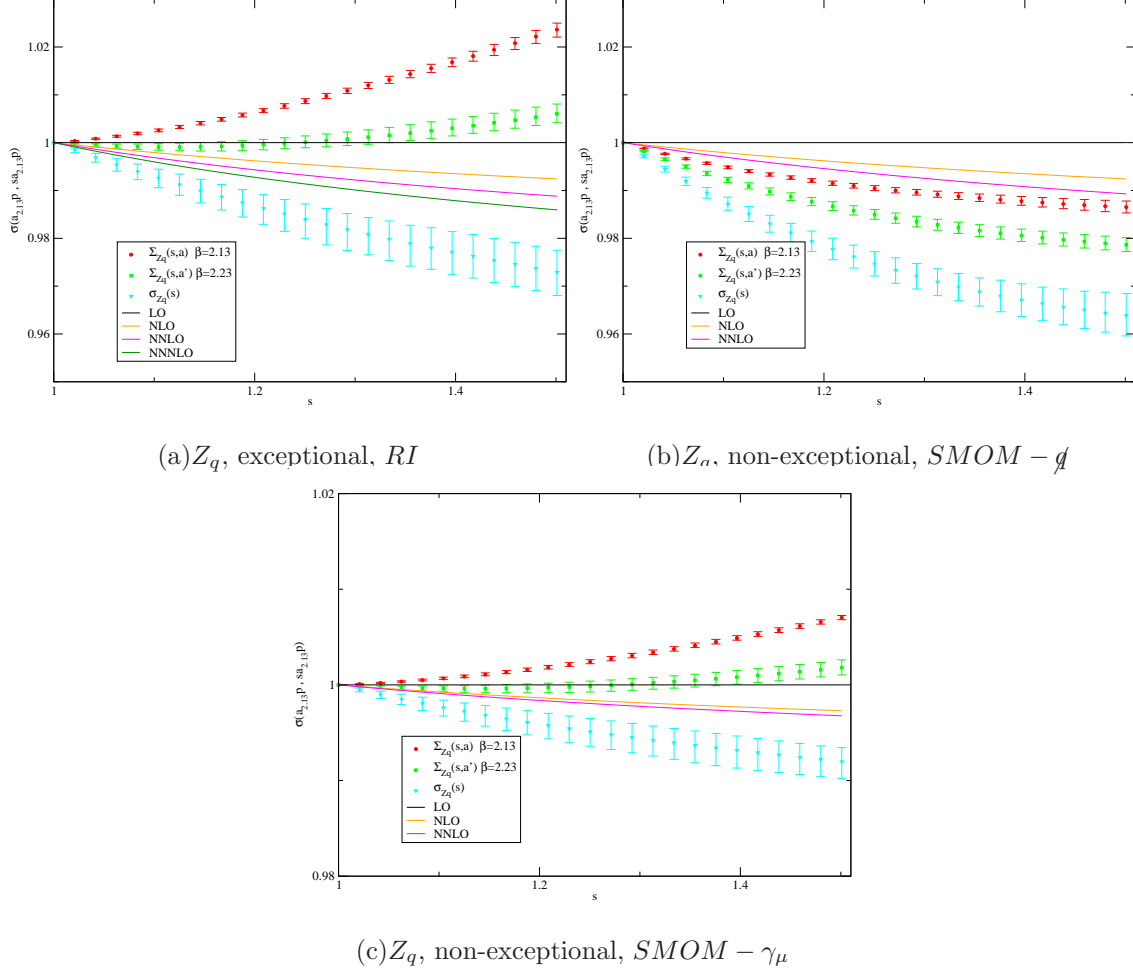


Figure 9: Quark field renormalization running from $\simeq 2$ GeV to $\simeq 3.0$ GeV in the three different schemes compared to the perturbative running in each scheme. The domain wall field normalisation depends on a localisation exponent $\alpha(p)$ that gives non-trivial lattice artefacts. The measured running can be seen to be wrong sign for the coarser lattice spacing, yet our controlled extrapolation to the continuum limit ends up same sign and somewhat enhanced relative to the perturbative four-loop exceptional anomolous dimension, and the two-loop non-exceptional anomolous dimension in the SMOM schemes.

in a number of schemes, as long as an unambiguous continuum limit can be defined, the Domain-Wall action will then produce the continuum scaling behaviour of Z_q and the other renormalization constants.

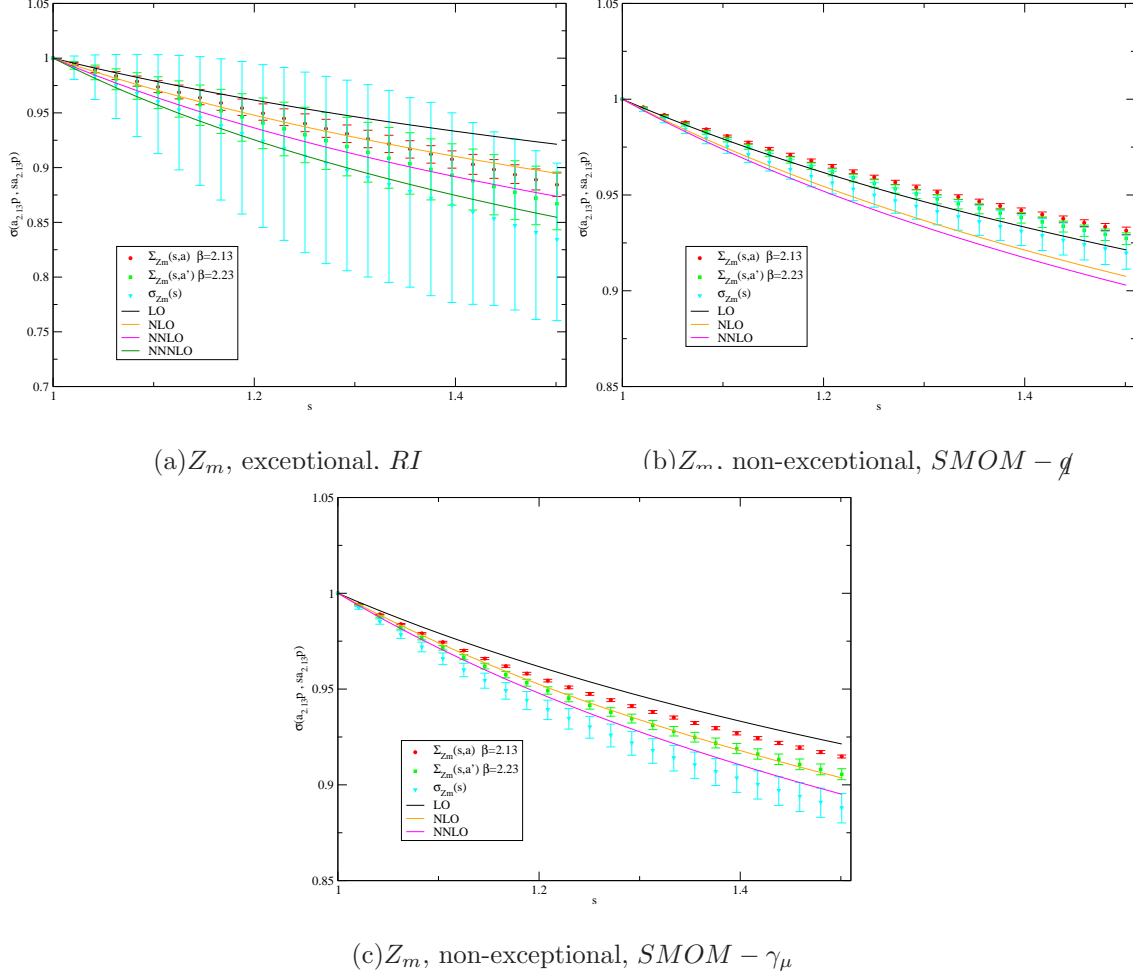


Figure 10: Quark mass renormalization running from $\simeq 2$ GeV to $\simeq 3.0$ GeV in the three different schemes compared to the perturbative running in each scheme.

V. CONCLUSIONS

We have introduced the use of twisted boundary conditions in off-shell renormalisation. This enables controlled Symanzik expansion of the relevant amplitudes and rigorous disentangling of lattice artefacts from perturbative truncation errors in the method.

We outlined a step scaling approach based on the scheme that will allow us to raise the scales at which perturbation theory is applied from around 2 GeV to at least around 5 GeV. The method has been demonstrated by taking the continuum limit of the first step scaling function in the process. The 5GeV upper scale is limited by the range over which our current matching based on the static potential is likely to be precise, and is the scale above which one should consider charm and bottom quark effects.

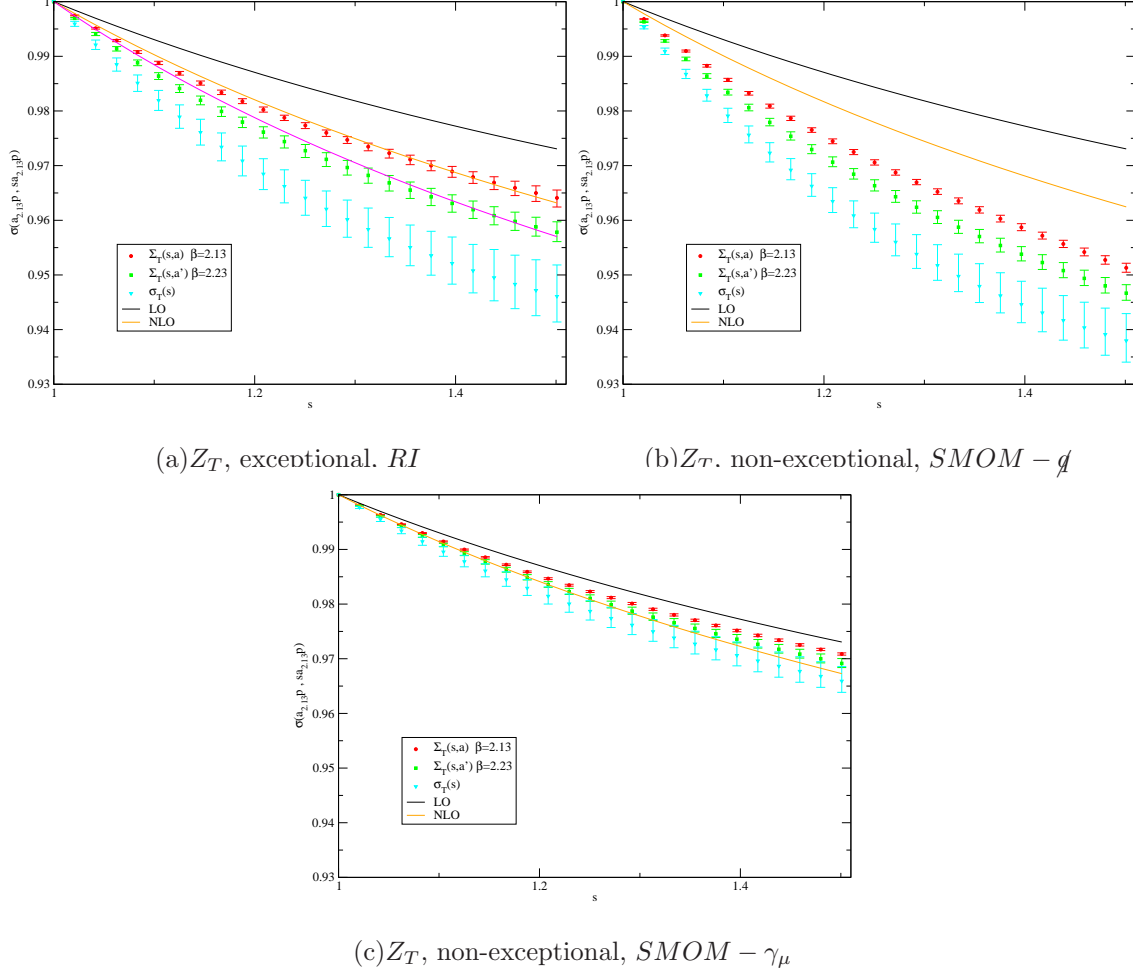


Figure 11: Tensor current renormalization running from $\simeq 2$ GeV to $\simeq 3.0$ GeV in the three different schemes compared to the perturbative running in each scheme.

The lattice spacing matching strategy will be the subject of further study, however, raising the scale at which, typically two or three loop, perturbation theory is applied for Rome-Southampton renormalisation for much important lattice phenomenology is already a significant step. For example, a naive estimate of an α^3 truncation error with $O(1)$ coefficient is reduced from 3% to under 1% by raising this scale to 5 GeV.

We plan to produce continuum limit scale evolution functions spanning the complete range of lattice operators covering the region 2-5 GeV. This includes all lattice bilinear and four quark operators, bilinear operators with covariant derivatives for structure functions and distribution amplitudes, and three quark operators relevant for proton decay matrix elements.

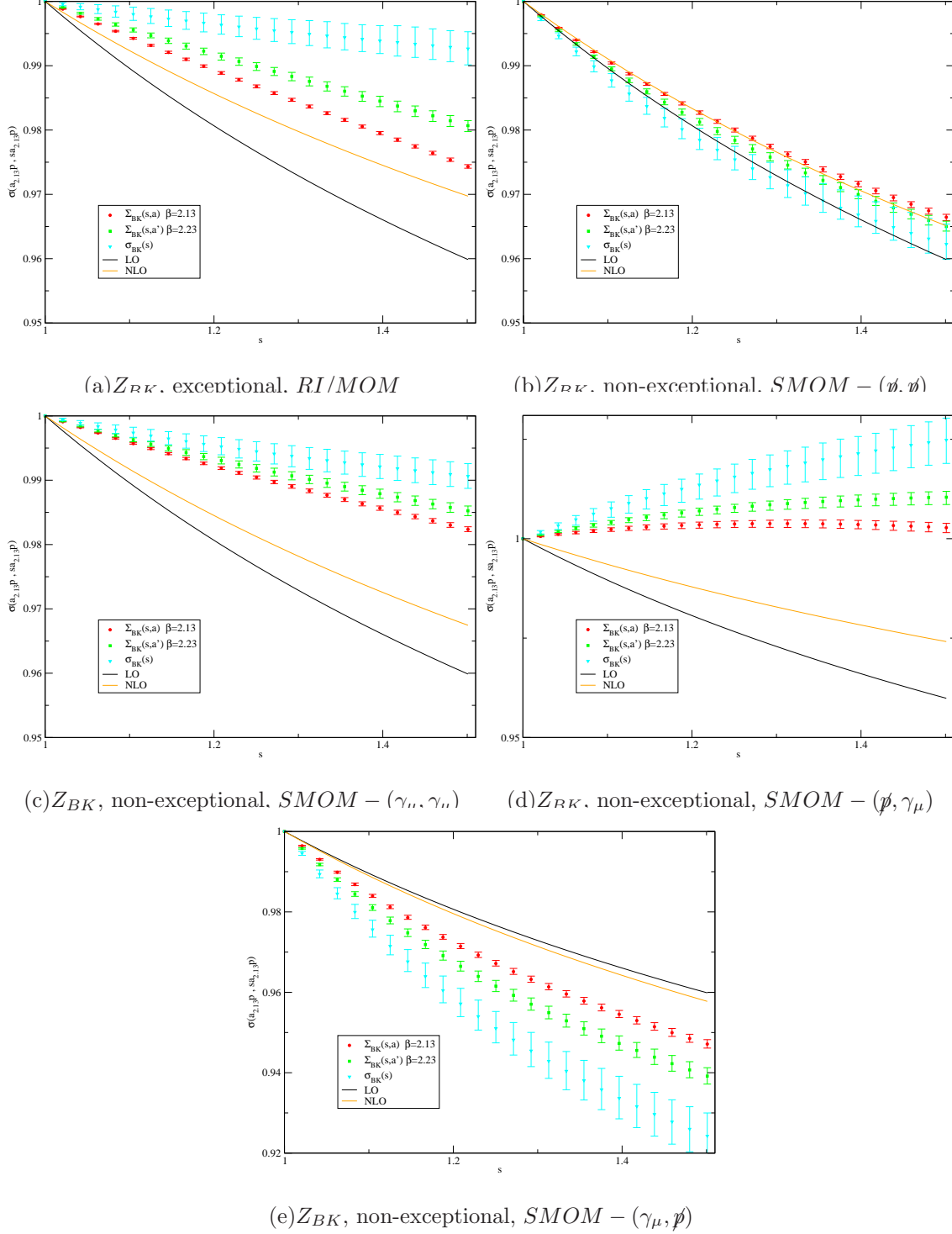


Figure 12: Quark field renormalization running from $\simeq 2$ GeV to $\simeq 3.0$ GeV in the three different schemes compared to the perturbative running in each scheme.

Obtaining the scaling functions in the continuum limit will enable calculations with any lattice action to raise the reference scale at which operators are quoted in \overline{MS} to be raised from 2 GeV to 5 GeV with substantial reduction in systematic errors.

VI. ACKNOWLEDGEMENTS

We would like to thank our colleagues in the RBC and UKQCD collaborations for many fruitful discussions, and particularly Yasumichi Aoki, Dirk Broemmelm, Norman Christ, Taku Izubuchi, Chris Kelly, Chris Sachrajda and Christian Sturm. We also wish to thank Luigi Del Debbio and David Lin for useful discussions. We particularly thank Chris Sachrajda and Christian Sturm for access to unpublished projectors and perturbative expressions for the SMOM schemes for the $VV + AA$ operator.

The software used includes: the CPS QCD codes http://qcdoc.phys.columbia.edu/chulwoo_index.html, supported in part by the US-DOE SciDAC program; the BAGEL [49] assembler kernel generator for many of the high-performance optimized kernels; and the UKHadron codes.

The authors were supported by PPARC grants PP/D000238/1 and PP/C503154/1. PAB acknowledges support from RCUK.

-
- [1] G. Martinelli, C. Pittori, C. T. Sachrajda, M. Testa and A. Vladikas, Nucl. Phys. B **445** (1995) 81 [arXiv:hep-lat/9411010].
 - [2] M. Gockeler *et al.*, Nucl. Phys. B **544** (1999) 699 [arXiv:hep-lat/9807044].
 - [3] V. Furman and Y. Shamir, Nucl. Phys. B **439** (1995) 54 [arXiv:hep-lat/9405004].
 - [4] Y. Iwasaki, Nucl. Phys. B **258** (1985) 141.
 - [5] T. Blum *et al.*, Phys. Rev. D **66** (2002) 014504 [arXiv:hep-lat/0102005].
 - [6] H. D. Politzer, Nucl. Phys. B **117** (1976) 397.
 - [7] P. Pascual and E. de Rafael, Z. Phys. C **12** (1982) 127.
 - [8] Y. Aoki *et al.*, Phys. Rev. D **78** (2008) 054510 [arXiv:0712.1061 [hep-lat]].
 - [9] C. Sturm, Y. Aoki, N. H. Christ, T. Izubuchi, C. T. C. Sachrajda and A. Soni, Phys. Rev. D **80** (2009) 014501 [arXiv:0901.2599 [hep-ph]].

- [10] RBC and UKQCD collaboration “Continuum limit of B_K from 2+1 Flavor Domain Wall QCD”, in preparation.
- [11] L. G. Almeida and C. Sturm, arXiv:1004.4613 [Unknown].
- [12] M. Gorbahn and S. Jager, arXiv:1004.3997 [Unknown].
- [13] Y. Aoki, “Non-perturbative renormalization in Lattice QCD”, PoS(Lattice 2009)012.
- [14] M. Luscher, R. Sommer, P. Weisz and U. Wolff, Nucl. Phys. B **413** (1994) 481 [arXiv:hep-lat/9309005].
- [15] M. Luscher, P. Weisz and U. Wolff, Nucl. Phys. B **359**, 221 (1991).
- [16] A. Bode *et al.* [ALPHA Collaboration], Phys. Lett. B **515** (2001) 49 [arXiv:hep-lat/0105003].
- [17] S. Sint, Nucl. Phys. B **451** (1995) 416 [arXiv:hep-lat/9504005].
- [18] S. Sint, Nucl. Phys. Proc. Suppl. **42** (1995) 835 [arXiv:hep-lat/9411063].
- [19] M. Luscher, R. Sommer, U. Wolff and P. Weisz, Nucl. Phys. B **389** (1993) 247 [arXiv:hep-lat/9207010].
- [20] M. Luscher, R. Narayanan, P. Weisz and U. Wolff, Nucl. Phys. B **384** (1992) 168 [arXiv:hep-lat/9207009].
- [21] E. Bilgici *et al.*, Phys. Rev. D **80** (2009) 034507 [arXiv:0902.3768 [hep-lat]].
- [22] Y. G. Zhestkov, PhD Thesis
- [23] Y. Zhestkov, arXiv:hep-lat/0101008.
- [24] K. Jansen *et al.*, Phys. Lett. B **372** (1996) 275 [arXiv:hep-lat/9512009].
- [25] P. A. Boyle, Nucl. Phys. Proc. Suppl. **129** (2004) 358 [arXiv:hep-lat/0309100].
- [26] P. F. Bedaque, Phys. Lett. B **593** (2004) 82 [arXiv:nucl-th/0402051].
- [27] G. M. de Divitiis, R. Petronzio and N. Tantalo, Phys. Lett. B **595** (2004) 408 [arXiv:hep-lat/0405002].
- [28] J. M. Flynn, A. Juttner and C. T. Sachrajda [UKQCD Collaboration], Phys. Lett. B **632** (2006) 313 [arXiv:hep-lat/0506016].
- [29] P. A. Boyle, J. M. Flynn, A. Juttner, C. T. Sachrajda and J. M. Zanotti, JHEP **0705** (2007) 016 [arXiv:hep-lat/0703005].
- [30] P. A. Boyle *et al.*, Phys. Rev. Lett. **100** (2008) 141601 [arXiv:0710.5136 [hep-lat]].
- [31] D. J. Antonio *et al.*, arXiv:hep-lat/0702026.
- [32] P. A. Boyle *et al.*, JHEP **0807** (2008) 112 [arXiv:0804.3971 [hep-lat]].
- [33] P. A. Boyle *et al.*, arXiv:1004.0886 [Unknown].

- [34] S. Necco and R. Sommer, Nucl. Phys. B **622** (2002) 328 [arXiv:hep-lat/0108008].
- [35] R. Sommer, Nucl. Phys. B **411** (1994) 839 [arXiv:hep-lat/9310022].
- [36] C. Allton *et al.* [RBC and UKQCD Collaborations], Phys. Rev. D **76** (2007) 014504 [arXiv:hep-lat/0701013].
- [37] D. J. Antonio *et al.* [RBC and UKQCD Collaborations], Phys. Rev. D **75** (2007) 114501 [arXiv:hep-lat/0612005].
- [38] D. J. Antonio *et al.* [RBC Collaboration and UKQCD Collaboration], Phys. Rev. D **77** (2008) 014509 [arXiv:0705.2340 [hep-lat]].
- [39] RBC-UKQCD Collaboration, “Continuum Limit Physics from 2+1 Flavor Domain Wall QCD”
In preparation
- [40] C. Allton *et al.* [RBC-UKQCD Collaboration], Phys. Rev. D **78** (2008) 114509 [arXiv:0804.0473 [hep-lat]].
- [41] K. G. Chetyrkin and A. Retey, Nucl. Phys. B **583**, 3 (2000) [arXiv:hep-ph/9910332].
- [42] J. A. Gracey, Nucl. Phys. B **662** (2003) 247 [arXiv:hep-ph/0304113].
- [43] A. J. Buras, M. Misiak and J. Urban, Nucl. Phys. B **586** (2000) 397 [arXiv:hep-ph/0005183].
- [44] M. Ciuchini, E. Franco, V. Lubicz, G. Martinelli, I. Scimemi and L. Silvestrini, Nucl. Phys. B **523** (1998) 501 [arXiv:hep-ph/9711402].
- [45] Y. Shamir, Nucl. Phys. B **406** (1993) 90 [arXiv:hep-lat/9303005].
- [46] G. S. Bali and P. Boyle, arXiv:hep-lat/0210033.
- [47] A. Hasenfratz, R. Hoffmann and F. Knechtli, Nucl. Phys. Proc. Suppl. **106** (2002) 418 [arXiv:hep-lat/0110168].
- [48] G. T. Fleming, arXiv:hep-lat/0403023.
- [49] P. A. Boyle, “The BAGEL assembler generator”, Computer Physics Communications **180**/12:2739 (2009) [doi:10.1016/j.cpc.2009.08.010]